The Astrophysical Journal, 677:L133–L136, 2008 April 20

RECONSTRUCTION OF THE 2007 MAY 22 MAGNETIC CLOUD: HOW MUCH CAN WE TRUST THE FLUX-ROPE GEOMETRY OF CMES?

Y. Liu,[1,2] J. G. Luhmann,[1] K. E. J. Huttunen,[1] R. P. Lin,[1] S. D. Bale,[1] C. T. Russell,[3] and A. B. Galvin[4]

Received 2008 January 22; accepted 2008 February 26; published 2008 March 24

ABSTRACT

Coronal mass ejections (CMEs) are often assumed to be magnetic flux ropes, but direct proof has been lacking. A key feature, resulting from the translational symmetry of a flux rope, is that the total transverse pressure as well as the axial magnetic field has the same functional form over the vector potential along any crossing of the flux rope. We test this feature (and hence the flux-rope structure) by reconstructing the 2007 May 22 magnetic cloud (MC) observed at *STEREO B*, *Wind*/*ACE*, and possibly *STEREO A* with the Grad-Shafranov (GS) method. The model output from reconstruction at *STEREO B* agrees fairly well with the magnetic field and thermal pressure observed at *ACE*/*Wind*; the separation between *STEREO B* and *ACE*/*Wind* is about 0.06 AU, almost half of the MC radial width. For the first time, we reproduce observations at one spacecraft with data from another well-separated spacecraft, which provides compelling evidence for the flux-rope geometry and is of importance for understanding CME initiation and propagation. We also discuss the global configuration of the MC at different spacecraft on the basis of the reconstruction results.

Subject headings: magnetic fields — solar wind — Sun: coronal mass ejections (CMEs)

Online material: color figure

1. INTRODUCTION

Coronal mass ejections (CMEs) have been investigated by remote sensing and in situ measurements for more than 30 years. One of the outstanding problems, however, is that their global morphology is still not well understood. Most models assume that CMEs are threaded by magnetic fields in the form of a helical flux rope (e.g., Chen 1996; Gibson & Low 1998; Lin & Forbes 2000). Correlation studies of CMEs at the Sun and 1 AU seem to support the flux-rope morphology (e.g., Krall et al. 2006; Yurchyshyn et al. 2006). The other possibility is that CMEs are spheromaks or plasmoids (e.g., Vandas et al. 1993a, 1993b), which appear to be consistent with the spherical shape often observed by coronagraphs. In the absence of coronal magnetic field measurements, however, none of these CME theories have been fully tested yet and it is hard to determine the CME geometry.

The magnetic structure can be inferred from in situ measurements of the interplanetary manifestations of CMEs (ICMEs). A force-free flux-rope model, as initially proposed by Goldstein (1983) for magnetic clouds (MCs), agrees with the measured fields and forms the basis for flux-rope fitting techniques (Marubashi 1986; Burlaga 1988; Lepping et al. 1990). Various flux-rope models, either force-free or non–force-free, circular or noncircular, have been developed since then in an effort to invert the global structure of MCs. However, the vast majority of in situ data analysis has been limited to a one-dimensional (1D) cut through the three-dimensional (3D) structure of ICMEs, and those flux-rope models involve many free parameters and assumptions, so the global morphology of ICMEs cannot be unambiguously determined. It should be stressed that a spherical plasmoid model can fit the observed MC fields as well as the cylindrical flux-rope model (Vandas et al. 1993a, 1993b). A question, crucial for both CME initiation and propagation in the heliosphere, thus arises regarding how well the flux-rope geometry can describe the CME structure.

A possible method to test the flux-rope structure relies on multipoint measurements, specifically to reproduce observations at one spacecraft using reconstruction of the flux rope with data from another well-separated spacecraft. Note that this approach is different from previous flux-rope fittings based on multispacecraft observations (e.g., Mulligan & Russell 2001; Riley et al. 2003; Liu et al. 2006b) in that it reproduces data at a second well-separated spacecraft with a model determined by observations from only one spacecraft. Certain requirements apply to the separation of the two spacecraft. At a small separation (e.g., *Wind* and *ACE*), the two spacecraft observe essentially the same structure, so a data-model comparison can hardly give strong constraints on the global structure. If the two spacecraft are too widely separated, the ambient solar wind conditions would be quite different; distortion of the ejecta by the ambient solar wind may not allow a practical data-model comparison. The spacecraft separation can also be limited by the calculation scheme (see § 2); models and observations indicate that the translational symmetry needed by the flux-rope reconstruction may not be valid for large spacecraft separations (e.g., Krall et al. 2006; Jackson et al. 2006). Therefore, the number of MCs that are suitable for this multispacecraft study is greatly restricted by the trade-off on the spacecraft separation. An optimum case would be such that the spacecraft separation is of the same order as or comparable to the flux-rope radial width.

The *STEREO* twin spacecraft, one preceding the Earth (*STEREO A*) and the other trailing behind (*STEREO B*), can provide multipoint in situ measurements of a single ICME together with spacecraft near L1. The 2007 May 22 MC is the first event observed at *STEREO B*, *Wind*/*ACE*, and possibly *STEREO A*, when these spacecraft are well but not too much separated. Figure 1 is an idealized 3D view of the MC modeled as a cylindrical flux rope with a diameter of 0.14 AU (obtained from the average speed times the MC duration) in RTN coordinates of *STEREO B* (in which *R* points from the Sun to the

[1] Space Sciences Laboratory, University of California, Berkeley, CA 94720; liuxying@ssl.berkeley.edu.

[2] State Key Laboratory of Space Weather, Chinese Academy of Sciences, Beijing 100080, China.

[3] Institute of Geophysics and Planetary Physics, University of California, Los Angeles, CA 90095.

[4] Institute for the Study of Earth, Oceans, and Space, University of New Hampshire, Durham, NH 03824.

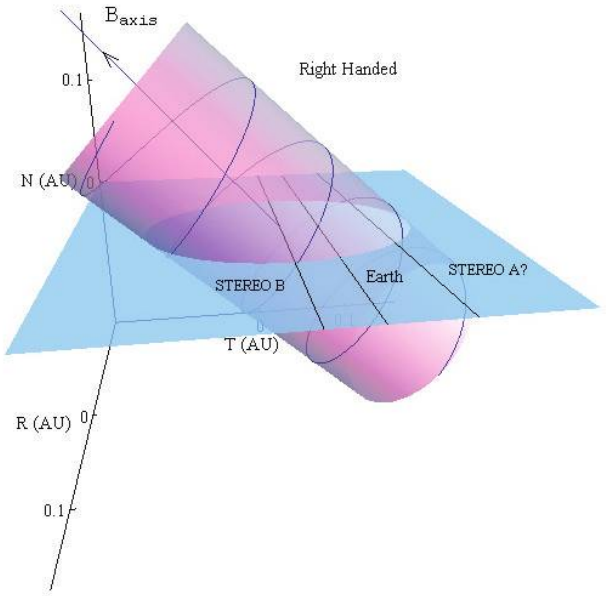

FIG. 1.—A 3D rendering of the MC in RTN coordinates of *STEREO B*. The arrow and the helical line indicate the orientation of the magnetic field. The horizontal lines denote radial crossings of the MC by the Earth and *STEREO* spacecraft in the solar equatorial plane (with *STEREO B* passing the MC axis).

spacecraft, *T* is parallel to the solar equatorial plane and points to the planet motion direction, and *N* completes the right-handed triad). Note that the Sun is at (−1, 0, 0) AU. The flux rope has an axis elevation angle of $\Theta \sim 50°$ and azimuthal angle of $\Phi \sim 270°$ (see § 2). The Earth and *STEREO* spacecraft, sitting roughly at 1 AU in the solar equatorial plane (see Table 1), would give in situ measurements of the MC along three lines as the MC radially passes these spacecraft. The longitudinal separation between *STEREO B* and the Earth is about 3° (see Table 1), which corresponds to a distance of 0.06 AU, comparable to the flux-rope radius (~0.07 AU). *STEREO A* is about 6° or 0.11 AU apart from the Earth. The configuration of these spacecraft provides a great opportunity to test the flux-rope model. In this Letter we reproduce observations at one spacecraft using data from another well-separated spacecraft for the first time, which reinforces the idea of the flux-rope geometry and is potentially important for understanding CME initiation, propagation, and the 3D structure of ICMEs.

2. OBSERVATIONS AND RECONSTRUCTION

Figure 2 shows the plasma and magnetic field measurements of the MC at *ACE* and *Wind*. The MC interval is identified by combining the enhanced helium/proton density ratio, depressed proton temperature (compared with the normal temperature expected from the observed speed), and strong magnetic fields with a large rotation. The boundaries also seem consistent with the discontinuities in the proton density, bulk speed, and the total thermal pressure *P*. Temperature measurements are not available

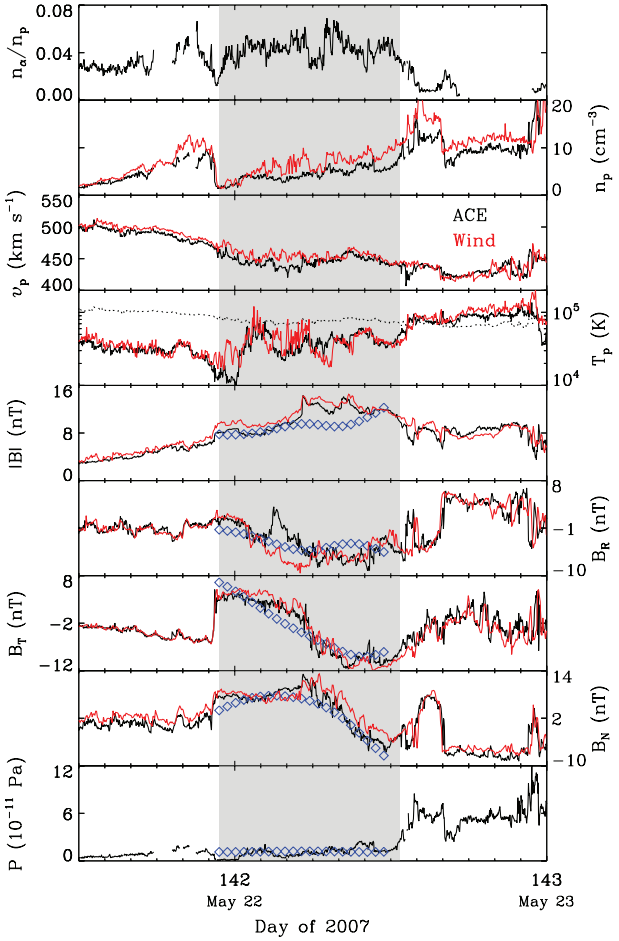

FIG. 2.—*ACE* (*black*) and *Wind* (*red*) data across the MC (*shaded region*). From top to bottom, the panels show the alpha/proton density ratio, proton density, bulk speed, proton temperature, magnetic field strength, magnetic field components in RTN coordinates, and the total thermal pressure. The dotted line denotes the expected proton temperature (*fourth panel*). Diamonds show the model output at *ACE*/*Wind* from the reconstruction at *STEREO B*. Note that they are not fittings of the *ACE*/*Wind* data.

for electrons and alpha particles, so the thermal pressure is calculated as $P = 4.5 n_p k_B T_p$ given the plasma charge neutrality and the observed density ratio $n_\alpha/n_p \simeq 0.05$, where k_B is the Boltzmann constant. We have assumed $T_e/T_p \sim 3$, $T_\alpha/T_p \sim 4$ as often observed in ICMEs (Liu et al. 2005, 2006a). As expected, *Wind* and *ACE* observe almost the same structure due to their small separation. Note that neither the *Wind* nor *ACE* data are time shifted. Comparison based on *Wind* and *ACE* observations, as discussed above, could not give constraints on the global structure of MCs.

Figure 3 displays *STEREO B* observations, together with *ACE* data for comparison. Note that the *ACE* data are time shifted by 5.3 hr. The MC boundaries at *STEREO B* are mainly determined from discontinuities in the magnetic field, proton density, and

TABLE 1
ESTIMATED PARAMETERS OF THE MC AT DIFFERENT SPACECRAFT

Spacecraft	Start (UT)	End (UT)	r[a] (AU)	θ[a] (deg)	ϕ[a] (deg)	Θ[b] (deg)	Φ[b] (deg)	Chirality
STEREO B	May 22 03:36	May 22 16:34	1.06	−2.6	161.8	57.8	262.8	R
ACE/Wind	May 21 22:19	May 22 12:43	1.01	−1.9	164.8	47.8	261.8	R
STEREO A	May 21 19:12	May 22 00:14	0.96	−1.1	170.7	37.6	230.2	R

[a] Heliographic inertial distance, latitude, and longitude of the spacecraft.
[b] Axis elevation and azimuthal angles in RTN coordinates.

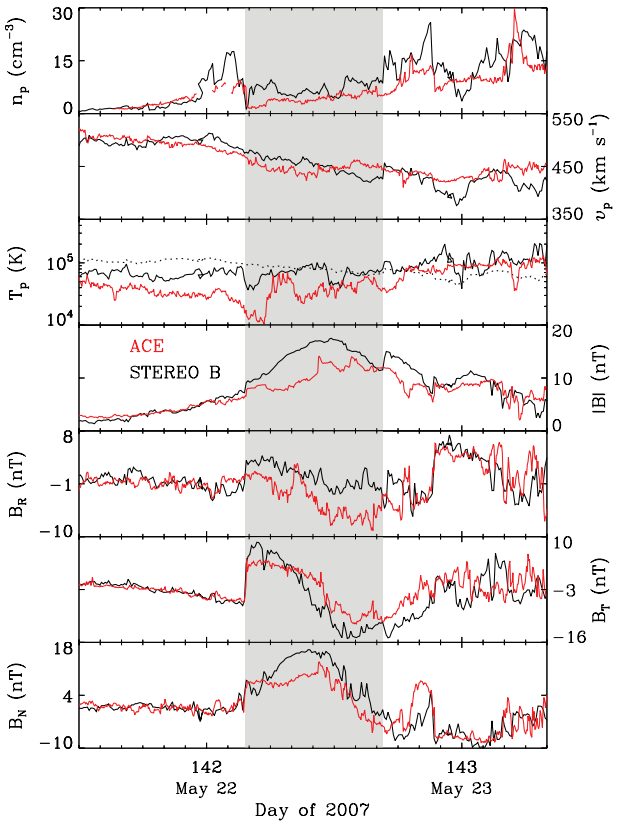

FIG. 3.—Same as Fig. 2, but for data at *STEREO B* (*black*) and *ACE* (*red*).

bulk speed, but they are also an output of the flux-rope reconstruction (see below). The *STEREO B* data within the MC, especially the magnetic field, are apparently different from the *ACE* data, indicating a sampling at a considerable distance from *ACE*/*Wind*. The ambient (particularly the upstream) field is very similar at *ACE* and *STEREO B*, so the spacecraft separation is not too large and enables a feasible model-data comparison. The magnetic field is stronger at *STEREO B* than at *ACE*, suggestive of a crossing closer to the MC axis.

We reconstruct the MC structure using the Grad-Shafranov (GS) technique (e.g., Hau & Sonnerup 1999; Hu & Sonnerup 2002). The advantage of this method is that it relaxes the force-free assumption and reconstructs the cross section of MCs without prescribing the geometry. Velocity and magnetic field measurements within the MC are transformed into a deHoffmann-Teller (HT) frame in which the electric field vanishes (e.g., Khrabrov & Sonnerup 1998). MHD equilibrium is obtained in this frame, i.e., $\boldsymbol{j} \times \boldsymbol{B} - \boldsymbol{\nabla} P = 0$, which can be reduced to the GS equation (e.g., Schindler et al. 1973; Sturrock 1994)

$$\frac{\partial^2 A}{\partial x^2} + \frac{\partial^2 A}{\partial y^2} = -\mu_0 \frac{d}{dA}\left(P + \frac{B_z^2}{2\mu_0}\right) \qquad (1)$$

by assuming a translational symmetry (i.e., $\partial/\partial z = 0$). Here $\boldsymbol{j}$ is the current density and μ_0 the permeability of vacuum. The magnetic field can be expressed as

$$\boldsymbol{B} = \left(\frac{\partial A}{\partial y}, -\frac{\partial A}{\partial x}, B_z\right) \qquad (2)$$

through the vector potential A. The thermal pressure P, the axial field B_z, and hence the transverse pressure $P_t = P + B_z^2/2\mu_0$ are

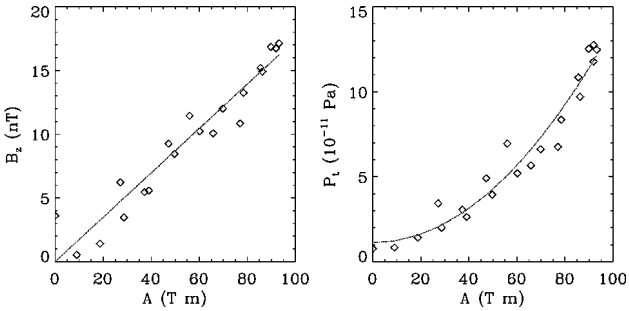

FIG. 4.—The axial magnetic field (*left*) and transverse pressure (*right*) as a function of A observed at *STEREO B*. The solid lines represent the best fits of the data (linear for B_z and second-order polynomial for P_t). [*See the electronic edition of the Journal for a color version of this figure.*]

functions of A alone (e.g., Schindler et al. 1973; Sturrock 1994). This feature, given by the translational symmetry of a flux rope, is key in testing the flux-rope geometry: if an MC is indeed a flux rope with a translational symmetry, then the behavior of P_t (and B_z) versus A should be the same at different spacecraft. The purpose of this work is mainly to test this point.

The axis orientation of an MC can be determined from the single-valued behavior of P_t over A (Hu & Sonnerup 2002). Application of this criterion to the plasma and magnetic field measurements within the MC at *STEREO B* yields an elevation angle $\Theta \simeq 57.8°$ and azimuthal angle $\Phi \simeq 262.8°$ in RTN coordinates (see Table 1). A flux-rope frame is then set up with the x-axis along a velocity $-\boldsymbol{v}_{\rm HT}$, the z-axis in the direction of the axial field, and the y-axis completing the right-handed triad. The HT-frame velocity, $\boldsymbol{v}_{\rm HT} \simeq (449, 0.4, -1.8)$ km s^{-1} (RTN), is obtained by minimizing the residual electric field (e.g., Khrabrov & Sonnerup 1998). The right-hand size of equation (1) is derived from the best fit of P_t versus A (in the flux-rope frame). Figure 4 shows B_z and P_t as a function of A observed at *STEREO B*. The vector potential along x is calculated from $A(x, 0) = -\int B_y dx'$. Small scatter around the linear (B_z) and second-order polynomial (P_t) fits indicates a well-ordered magnetic structure. The best fits should hold over the entire cross section as required by the flux-rope geometry; we will evaluate this feature using a data-model comparison (see below).

Equation (1) can then be solved for A in a rectangular domain using *STEREO B* observations as spatial initial values. Away from the observation baseline the vector potential A is calculated based on its second-order Taylor expansion with respect to y. Note that this integration is intrinsically a Cauchy problem and numerical singularities may arise after a certain number of steps; in general, the integration cannot go further than half of the radial width from the observation line. Differentiation of A gives B_x and B_y through equation (2), while the axial field B_z and the thermal pressure P can be derived from the best fits (shown in Fig. 4) with the calculated A. The recovered cross section is shown in Figure 5. The contours represent nested helical field lines projected onto the cross section. The field configuration is right-handed, as can be seen from the transverse fields along the trajectory of *STEREO B*. The maximum B_z field (presumably at the axis) is very close to the trajectory with an impact parameter ~0.002 AU, in good agreement with observations (see Fig. 3). The path of *ACE*/*Wind*, rotated into the flux-rope frame, is about 0.05 AU away from *STEREO B* in the cross section (1/3–1/2 of the MC radial width). For any point along this line, the vector magnetic field as well as the thermal pressure can be obtained from the solutions of equation (1). If the model output at *ACE*/*Wind* agrees with the data, then the flux-rope structure as well as the reconstruction scheme can be well verified.

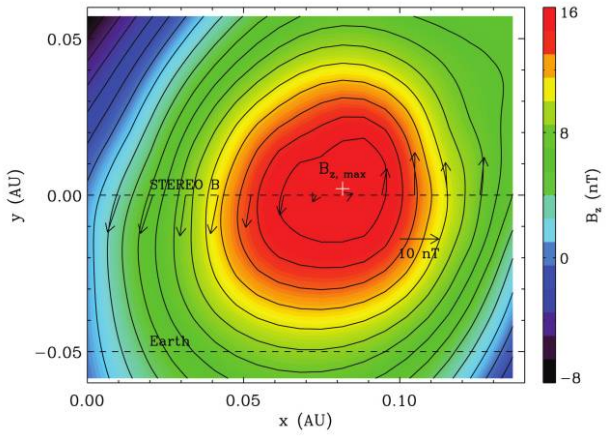

FIG. 5.—Reconstructed cross section of the MC at *STEREO B*. Black contours show the distribution of the vector potential and the color shading indicates the value of the axial field. The dashed lines mark the trajectories of *STEREO B* and the Earth, respectively. The arrows denote the direction and magnitude of the observed magnetic fields projected onto the cross section. The location of the maximum axial field is indicated by the plus sign.

The comparison between data and model output at *ACE*/*Wind* is shown in Figure 2 after a transformation from the flux-rope frame into RTN coordinates. The agreement is generally good for both the magnetic field and the thermal pressure. Including the thermal pressure is a unique capability of the GS method, which makes the thermal pressure comparison available. Deviations are also seen but mainly around the dynamical features inside the MC (most visible from the field magnitude and B_R). These dynamical features are not in MHD equilibrium assumed in the reconstruction. Numerical errors could also contribute to the deviations. The overall trends, however, are well reproduced. It should be stressed that the reconstruction, in particular the output of B_z and P, is largely based on the best fits shown in Figure 4. The good data-model agreement justifies the central point that the transverse pressure and the axial field are functions of A alone; combined with the helical fields in Figure 5, this verified feature shows that the MC is a flux rope.

We also reconstruct the MC separately at *STEREO A* and *ACE*/*Wind*. Table 1 lists the times, locations, estimated axis orientations, and field chiralities. These spacecraft were very close to the solar equatorial plane and seemed to observe the MC successively, consistent with their heliocentric distances. The axis orientation is similar at the four spacecraft but with discernible variations. The MC is right-handed at all the spacecraft, as illustrated in Figure 5. It is not clear whether *STEREO A* observed this event, given a radial width of ~0.06 AU (5 hr), which is substantially smaller than at *STEREO B* and *ACE*/*Wind*; the timing, axis orientation and field chirality, however, all seem consistent. It is likely that *STEREO A* observed the flank of the MC (still part of the MC; see Fig. 1). See more detailed discussions of *STEREO A* observations by Huttunen et al. (2008). The radial width is nearly the same at *STEREO B* and *ACE*/*Wind* (0.14 and 0.15 AU, respectively). The observed radial widths and the spacecraft configuration reveal a flattened cross section, consistent with the finding of Liu et al. (2006b); if the MC is indeed observed at *STEREO A*, then half of the transverse size (from *STEREO B* to *STEREO A* along y since *STEREO B* crossed the axis) is at least 0.16 AU and comparable to the radial width, so the aspect ratio may be around 2 : 1 or even larger. Note that *ACE*/*Wind* is at a considerable distance from the flux-rope axis (see Fig. 5); reconstruction using *ACE*/*Wind* data cannot match observations at *STEREO B* as well as what we did in Figure 2, which is probably restricted by the integration scheme of the GS method (an intrinsic Cauchy problem).

3. SUMMARY

We have tested the flux-rope geometry of CMEs by reconstructing the 2007 May 22 MC observed at *STEREO B*, *ACE*/*Wind*, and likely *STEREO A* with the GS technique. The pivotal feature of a flux rope we base on is that the total transverse pressure (P_t) and the axial magnetic field (B_z) are functions of the vector potential only. The vector magnetic fields and the thermal pressure resulting from reconstruction with *STEREO B* data generally match *ACE*/*Wind* observations. The separation between *ACE*/*Wind* and *STEREO B* is about 0.06 AU, which translates to a distance of ~0.05 AU in the MC cross section (see Fig. 5) and ~0.04 AU along the MC (see Fig. 1). If the MC were a spherical plasmoid as suggested by Vandas et al. (1993a, 1993b) the magnetic field would be totally different after a translational distance of 0.06 AU (almost 1/2 of the radial width). Consequently, the multispacecraft MC data reported here cannot be simultaneously fitted using a plasmoid model, although the plasmoid model may fit data at a single spacecraft. Given such a large spacecraft separation (as compared with the MC radial width) and the successful data-model comparison, we conclude that the single-valued behaviors of P_t and B_z and thus the flux-rope geometry are well validated, at least for the current MC. The reconstruction also shows that the MC is highly flattened, probably due to the solar wind radial expansion as found by Liu et al. (2006b).

The research was supported by the *STEREO* project under grant NAS5-03131. Y. L. thanks Q. Hu of UC Riverside for helpful discussion. We acknowledge the use of *ACE* and *Wind* data. This work was also supported in part by grant NNSFC 40621003.

REFERENCES

Burlaga, L. F. 1988, J. Geophys. Res., 93, 7217
Chen, J. 1996, J. Geophys. Res., 101, 27499
Gibson, S. E., & Low, B. C. 1998, ApJ, 493, 460
Goldstein, H. 1983, in Solar Wind Five, ed. M. Neugebauer (Washington, DC: NASA), 731
Hau, L.-N., & Sonnerup, B. U. Ö. 1999, J. Geophys. Res., 104, 6899
Hu, Q., & Sonnerup, B. U. Ö. 2002, J. Geophys. Res., 107, 1142
Huttunen, K. E. J., et al. 2008, Geophys. Res. Lett., submitted
Jackson, B. V., et al. 2006, J. Geophys. Res., 111, A04S91
Khrabrov, A. V., & Sonnerup, B. U. Ö. 1998, in Analysis Methods for Multi-Spacecraft Data, ed. G. Paschmann & P. W. Daly (Noordwijk: ESA), 221
Krall, J., et al. 2006, ApJ, 642, 541
Lepping, R. P., et al. 1990, J. Geophys. Res., 95, 11957
Lin, J., & Forbes, T. G. 2000, J. Geophys. Res., 105, 2375
Liu, Y., et al. 2005, Planetary Space Sci., 53, 3
———. 2006a, J. Geophys. Res., 111, A01102 (doi:10.1029/2005JA011329)
———. 2006b, J. Geophys. Res., 111, A12S03 (doi:10.1029/2006JA011890)
Marubashi, K. 1986, Adv. Space Res., 6, 335
Mulligan, T., & Russell, C. T. 2001, J. Geophys. Res., 106, 10581
Riley, P., et al. 2003, J. Geophys. Res., 108, 1272
Schindler, K., et al. 1973, Plasma Phys., 15, 1165
Sturrock, P. A. 1994, Plasma Physics: An Introduction to the Theory of Astrophysical, Geophysical and Laboratory Plasmas (New York: Cambridge Univ. Press), 209
Vandas, M., et al. 1993a, J. Geophys. Res., 98, 11467
———. 1993b, J. Geophys. Res., 98, 21061
Yurchyshyn, V., et al. 2006, Sol. Phys., 239, 317